Author Manuscript

Author Manuscript

Author Manuscript

Author Manuscript

HHS Public Access

Author manuscript

J Mol Cell Cardiol. Author manuscript; available in PMC 2020 October 01.

Published in final edited form as:

J Mol Cell Cardiol. 2019 October ; 135: 1–9. doi:10.1016/j.yjmcc.2019.07.013.

Dynamic Palmitoylation Regulates Trafficking of K Channel Interacting Protein 2 (KChIP2) across Multiple Subcellular Compartments in Cardiac Myocytes

Akshay Murthy[1,*], **Samuel Workman**[1,*], **Min Jiang**[2], **Junping Hu**[1], **Ismat Sifa**[1], **Tytus Bernas**[3], **Wanchun Tang**[4], **Isabelle Deschenes**[5], **Gea-Ny Tseng**[1]

[1]Department of Physiology and Biophysics Virginia Commonwealth University Richmond, VA 23298

[2]Institute of Medicinal Biotechnology Chinese Academy of Medical Sciences and Peking Union Medical College Beijing 100050, China

[3]Department of Anatomy and Neurobiology Virginia Commonwealth University Richmond, VA 23298

[4]Weil Institute of Emergency and Critical Care Research Virginia Commonwealth University, Richmond, VA 23298

[5]Medicine, Physiology and Biophysics, and Biomedical Engineering The MetroHealth System, Case Western Reserve University Cleveland, OH 44109

Abstract

Background: K channel interacting protein 2 (KChIP2), initially cloned as Kv4 channel modulator, is a multi-tasking protein. In addition to modulating several cardiac ion channels at the plasma membrane, it can also modulate microRNA transcription inside nuclei, and interact with presenilins to modulate Ca release through RyR2 in the cytoplasm. However, the mechanism regulating its subcellular distribution is not clear.

Objective: We tested whether palmitoylation drives KChIP2 trafficking and distribution in cells, and whether the distribution pattern of KChIP2 in cardiac myocytes is sensitive to cellular milieu.

Methods: We conducted imaging and biochemical experiments on palmitoylatable and unpalmitoylatable KChIP2 variants expressed in COS-7 cells and in cardiomyocytes, and on native KChIP2 in myocytes.

For correspondence: Gea-Ny Tseng, PhD, Department of Physiology & Biophysics, Virginia Commonwealth University, 1101 E. Marshall Street, Sanger Hall, 3-042a, Richmond, VA 23298, gtseng@vcu.edu, (804)827-0811.

*Co-first authors

DISCLOSURES

None

Publisher's Disclaimer: This is a PDF file of an unedited manuscript that has been accepted for publication. As a service to our customers we are providing this early version of the manuscript. The manuscript will undergo copyediting, typesetting, and review of the resulting proof before it is published in its final citable form. Please note that during the production process errors may be discovered which could affect the content, and all legal disclaimers that apply to the journal pertain.

Author Manuscript Author Manuscript Author Manuscript Author Manuscript

Results: In COS-7 cells, palmitoylatable KChIP2 clustered to plasma membrane, while unpalmitoylatable KChIP2 exhibited higher cytoplasmic mobility and faster nuclear entry. The same differences in distribution and mobility were observed when these KChIP2 variants were expressed in cardiac myocytes, indicating that the palmitoylation-dependent distribution and trafficking are intrinsic properties of KChIP2. Importantly, acute stress in a rat model of cardiac arrest/resuscitation induced changes in native KChIP2 resembling those of KChIP2 depalmitoylation, promoting KChIP2 nuclear entry.

Conclusion: The palmitoylation status of KChIP2 determines its subcellular distribution in cardiac myocytes. Stress promotes nuclear entry of KChIP2, diverting it from ion channel modulation at the plasma membrane to other functions in the nuclear compartment.

Keywords

Palmitoylation; protein trafficking; cardiac stress; potassium channel

INTRODUCTION

KChIP1-KChIP3 can enhance surface expression of Kv4.2 or Kv4.3 channels and modulate their gating kinetics [1], establishing their role as major auxiliary subunits of transient outward (I_{to}) or A-type (I_A) channels in the heart and the brain, respectively. It was recognized that KChIP3 and two other previously characterized proteins are encoded by the same gene. These two proteins are DREAM (downs tream regulatory element antagonist modulator, a Ca-sensitive transcription repressor localized in nuclei), and calsenilin (presenilin modulator, localized in cytoplasm/endoplasmic reticulum) [2]. More recent studies showed that KChIP2, the only KChIP expressed in the heart, can also multi-task [3–7]. KChIP2 can modulate miRNA transcription [4]. It may interact with presenilin-1 in the sarcoplasmic reticulum [8] to modulate Ca release through ryanodine receptor 2 (RyR2) [5]. Finally, KChIP2 can modulate the surface expression and/or function of not only Kv4 channels, but also Cav1.2 [7] and Kv1.5 [6]. These observations indicate that both KChIP2 and KChIP3 can serve different functions depending on their subcellular locations. However, it is not clear how the subcellular distribution of KChIP2 or KChIP3 is determined and modulated.

It has been shown that several proteins use the reversible process of S-palmitoylation to control their shuttle between cytoplasm/plasma membrane (PM) and nucleus [9–11]. S-Palmitoylation is a reversible form of post-translational modification, mediated by palmitoyl acyl transferases (linking a long saturated fatty acyl chain, most commonly palmitoyl, to the thiol group of cysteine ‘Cys’ in proteins) and palmitoyl thioesterases (depalmitoylating substrates). Palmitoylation of soluble proteins promotes their binding to cellular membranes, while depalmitoylation releases these proteins from membrane anchors. Both KChIP2 (long splice variants, see below) and KChIP3 can be S-palmitoylated at a double Cys motif in their N-terminal domain [12].

In this study, we tested the possibility that KChIP2 uses the mechanism of reversible depalmitoylation/repalmitoylation to control its distribution between nucleus and cytoplasm/PM. We further examined how the palmitoylation status of KChIP2 affects its

Author Manuscript Author Manuscript Author Manuscript Author Manuscript

mobility within and between these subcellular compartments, and how acute stress imposed on the heart could alter its distribution.

MATERIALS AND METHODS

1. Human heart samples and animal models

Frozen de-identified human heart samples were obtained from Duke Human Heart Repository, Duke University, associated with IRB Pro00084269 and Pro00005621.

The use of rat, dog and guinea pig animal models was reviewed and approved by IACUC of VCU (AM10294). We used male Sprague-Dawley rats weighing 450–550 g, mongrel dogs of either sex 2–3 years old, and male guinea pigs weighing 450–500 g.

2. Molecular constructs

Human KChIP2.2-mCherry and mCherry-KChIP2.2 were purchased from GeneCopoeia. C45A/C46A mutation and mCherry-KChIP2.6 were created in house and confirmed by DNA sequencing.

3. COS-7 and HEK293 cell culture and transfection

Cells were maintained in DMEM supplemented with 10% fetal calf serum, nonessential amino acids and penicillin/streptomycin at 36°C in a humidified CO_2 incubator. Cells were plated on matrigel-coated dishes or coverslips, and transfected with cDNA (0.2–0.4 ug/ml) assisted by lipofectamine 2000. Cells were cultured for another 16–36 hr before experiments.

4. Rat model of cardiac arrest/resuscitation (CAR)

The procedure was reviewed and approved by institutional IACUC, and described previously [13]. Briefly, ventricular fibrillation (VF) was induced by burst pacing of right ventricle. After 8 min of VF without mechanical ventilation, resuscitation was attempted with mechanical chest compressor. Heart was harvested and immediately used for myocyte isolation.

5. Myocyte isolation, culture, and adenoviral infection

The procedures have been described previously [14]. Briefly, myocytes were isolated using a combination of collagenase digestion and mechanical trituration. Myocytes were plated on laminin- or matrigel-coated dishes or coverslips and cultured in medium 199, supplemented with L-carnitine (5 mM), creatine phosphate (5 mM), taurine (5 mM), BSA (0.2%), fetal calf serum (2%), cytochalasin D (0.2 uM, to stabilize actin filaments and preserve t-tubules during myocyte culture [15]), and penicillin/streptomycin in 36°C humidified incubator, and incubated with adenovirus carrying KChIP2.2-mCherry (1×10^7 plague-forming unit ‘PFU’ per ml) for 24 hr before experiments.

5. Detection of KChIP2 palmitoylation

The procedures are described in Fig. S1. Cells transfected with KChIP2.2-mCherry were incubated with palmitate-alkyne (100 μM) at 36°C overnight. KChIP2-mCherry was

Author Manuscript Author Manuscript Author Manuscript Author Manuscript

immunoprecipitated with RFP nanobody (Nb) beads. Protein-bound beads were 'clicked' [16] with azide-conjugated biotin. Protein-bound and clicked beads were incubated with hydroxylamine (HA, 0.75 M, pH 7.4) or with Tris (0.75 M) at room temperature for 1 hr before elution, followed by immunoblot experiments.

Subcellular distribution pattern of palmitoylated KChIP2.2-mCherry was detected by combining palmitate-alkyne labeling, click reaction with azide-conjugated biotin, and *in situ* proximity ligation amplification in a process termed 'Palm-PLA' [17] using Duolink fluorescence assay kit (Sigma Millipore). Subcellular distribution pattern of unpalmitoylated KChIP2.2-mCherry was detected by a procedure (Unpalm-PLA) similar to the above except that free thiol side chains of Cys were biotinylated (Fig. S1B, panel (c)).

6. Cytosolic/membrane and nuclear fractionation of ventricular myocardium

This was done using NE-PER nuclear and cytoplasmic extraction kit (Thermo Fisher) according to manufacturer's instruction.

7. Immunoblot experiments

This has been described previously [14]. Briefly, proteins were fractionated by SDS polyacrylamide gel electrophoresis, and transferred to PVDF membrane. The PVDF membrane was incubated with primary Ab overnight at 4°C. Membrane was incubated with horse radish peroxidase-conjugated secondary Ab, and immunoreactive bands were visualized with enhanced chemiluminescence kit using FluorChem M imager. Band intensities were quantified using AlphaView SA and numerical data were exported to Excel for processing.

8. Imaging experiments and data analysis

To image fixed cells, cells were fixed, permeabilized (0.1% Triton-X100, 10 min), incubated with Abs (for immunofluorescence), and mounted on glass slides with ProLong Diamond antifade mountant (Molecular Probes). Cells were imaged with Zeiss 710 confocal microscope using 63x (COS-7) or 40x (myocytes) oil immersion objective. Fluorophores were sequentially excited by laser of 405 nm (DAPI and Hoechst dye), 488 nm (Alexa488 or GFP), 561 nm (Alexa568 or mCherry), and 633 (Alexa647). Pixel contents in regions of interest (ROIs), calculated as (mean pixel value in ROI –background)x(area of ROI), were used to calculate % pixel contents in different ROIs of a cell.

To image live cells, cells were plated on microwell dishes (MatTek), and transfected with cDNA or infected with adenovirus. After staining nuclei with Hoechst dye, COS-7 cells were imaged in phenol-red free, 25 mM HEPES DMEM supplemented with 10% FCS at 37°C. Live myocytes were imaged in normal Tyrode's supplemented with 10% FCS and 10 uM blebbistatin (to prevent contractile activity) at 37°C. In fluorescence loss in photobleaching (FLIP) experiments, mean pixel values in delineated ROIs were reported by Zeiss software and exported to Excel for processing.

9. Antibodies

The Abs used are listed in on-line Table S1.

Author Manuscript Author Manuscript Author Manuscript Author Manuscript

10. Statistical analysis

For comparison among three or more groups, SigmaStat 4.0 was used to perform one-way ANOVA analysis. If the p value was less than 0.01, Dunn's all-pairwise test or test against a reference group was used to detect statistically significant differences among the groups.

RESULTS

Native KChIP2 in cardiac myocytes exhibits divergent distribution patterns

Despite the important roles played by KChIP2 in cardiac electrical and contractile activity [4–7, 18], studies on its distribution pattern in cardiac myocytes are sparse and the results appear divergent. In human ventricular myocytes, a pan-KChIP Ab detected striation signals in the cytoplasm and puncta inside nuclei [19]. In rat ventricular myocytes, a KChIP2-specific mAb revealed KChIP2-positive vesicles in the cytoplasm and puncta inside nuclei [4]. A third Ab detected prominent signals along the lateral surface, but not in the cytoplasm, of rat ventricular myocytes [20]. These divergent patterns cannot be explained solely by differences in the Ab used in immunofluorescence detection or the species examined. Fig. 1A depicts KChIP2 immunofluorescence detected by the KChIP2-specific mAb mentioned above [4] in three canine ventricular myocytes. KChIP2 is in prominent striations in cell (1), in striations plus vesicles in cell (2), and mainly in vesicles in cell (3). In all three myocytes, KChIP2 is also detected in perinuclear Golgi apparatus, as well as puncta in the chromatin-free space of nuclei (close-up view in Fig. 1B). Immunoblot confirmed the presence of native KChIP2 protein in both cytosolic/membrane and nuclear fractions of dog and non-failing human hearts (Fig. 1C). These observations suggest that KChIP2 can assume dynamic distribution patterns in cardiac myocytes.

Palmitoylation is a major determinant of KChIP2 distribution between plasma membrane and nucleus

KChIP2 is a cytosolic soluble protein that can be S-palmitoylated at C45/C46 [12]. S-palmitoylation is a reversible process mediated by palmitoylating and depalmitoylating enzymes. It has been shown that a number of S-palmitoylatable proteins use depalmitoylation/repalmitoylation cycles to control their distribution between cytoplasm/PM and nucleus [9–11]. To test whether KChIP2 uses the same mechanism to control its subcellular distribution, we conducted experiments in COS-7 cells expressing palmitoylatable and unpalmitoylatable KChIP2 variants (KChIP2.2 and KChIP2.6, respectively, Fig. 2A). We also made an unpalmitoylatable KChIP2.2 mutant (C45A/C46A) [12]. These KChIP2 variants were tagged with mCherry, to allow their detection without any Ab. Three observations indicate that the mCherry tag did not interfere with KChIP2's function. First, KChIP2.2-mCherry is S-palmitoylatable (Fig. 2B). Second, KChIP2.2 having mCherry fused to either the N- or C-terminus (mCherry-KChIP2.2 and KChIP2.2-mCherry) exhibited the same distribution pattern distinctly different from that of unpalmitoylatable variants (Fig. 2C). Third, all mCherry-tagged KChIP2 variants were capable of accelerating recovery of K4.3 channels from inactivation, the signature function of KChIP2 (Fig. S2).

There are quantitative differences in the nucleus-PM distribution pattern between palmitoylatable and unpalmitoylatable KChIP2 variants (Fig. 2C): the former group had a

Author Manuscript Author Manuscript Author Manuscript Author Manuscript

higher level at PM but lower in nucleus than the latter group. Inhibiting palmitoylation by incubating cells with a palmitoylation inhibitor, 2-bromopalmitate [21] (2BP) switched the distribution pattern of palmitoylatable KChIP2 variants to that of unpalmitoylatable ones, but did not have detectable effects on the latter group.

Due to the reversible nature of S-palmitoylation, there were two pools of palmitoylatable KChIP2.2-mCherry in cells: palmitoylated and unpalmitoylated. To probe whether these two pools of KChIP2.2-mCherry were different in their subcellular distribution, we combined the techniques of *in situ* proximity ligation amplification (PLA) and biotinylation of either palmitoylated thiol side chains, or free (unpalmitoylated) thiol side chains. These two procedures, Palm-PLA and Unpalm-PLA, are described in Fig. S1B. Fig. 3A depicts the distribution patterns of PLA signals of palmitoylated and unpalmitoylated pools, along with immunofluorescence (IF) signals of total KChIP2.2-mCherry. The PLA signals of both pools of KChIP2.2-mCherry were present in the cytoplasm. Palmitoylated KChIP2.2-mCherry was largely excluded from the nucleoplasm, despite the presence of KChIP2.2-mCherry IF in the same region. On the other hand, unpalmitoylated KChIP2.2-mCherry was abundantly present in the nucleoplasm. The distinction between the two pools of KChIP2.2-mCherry is best seen in the XZ-plane views. To compare their nuclear distribution statistically, we quantified the percentages of Palm- and Unpalm-PLA pixel contents in nuclear regions normalized by the percentages of IF pixel contents in the same region. This was done on z-projections of sum of fluorescence intensities across the whole cell thickness. PLA pixels in the thin cytoplasm above and beneath the nuclei would contribute to the PLA pixel contents in nuclear regions. Given this caveat, the amount of unpalmitoylated pool inside nuclei was much higher than that of palmitoylated pool (Fig. 3B).

Palmitoylation influences mobility of KChIP2 in cytoplasm and between cytoplasm and nucleus

One important role of palmitoylation is to control protein trafficking among subcellular compartments [22]. Figs. 2 and 3 together show that palmitoylated KChIP2 is enriched at PM but excluded from the nucleus, while unpalmitoylated KChIP2 is low at PM but present inside the nucleus. To test whether this differential distribution at steady-state reflects altered trafficking behavior, we quantified their mobility in live cell photobleaching experiments. Pilot experiments showed that the conventional approach, fluorescence recovery after photobleaching, was not suitable: because of the fast movement of soluble KChIP2 in cytoplasm we could not bleach KChIP2.2-mCherry in a specific area without seriously bleaching its signals in other areas of the same cell. Therefore, we used an alternative approach, fluorescence loss in photobleaching (FLIP). Fig. 4A illustrates the concept. The fluorescence intensities in a selected area and its immediate surrounding (near neighbor) were monitored with low-intensity (≤ 1% power) laser scan once every 15 s. After the baseline data were obtained, a strong (100% power) laser pulse was applied to the central area after every low-intensity laser scan. This sequence was repeated multiple times, during which the fluorescence intensities in both areas declined gradually due to fluorescent KChIP2 moving from unbleached neighborhood to the directly bleached area. The difference in the rates of decline in fluorescence intensity between the two compartments reflects the protein's mobility between them.

Author Manuscript Author Manuscript Author Manuscript Author Manuscript

To illustrate the utility of this approach, we coexpressed Kv4.3-GFP (membrane embedded tetramer, 402 kDa) and free mCherry (cytosolic monomer, 26.7 kDa) in COS-7 cells and applied FLIP to compare their mobility in the same cytoplasmic region. Fig. 4B shows that while mCherry's fluorescence intensity declined at the same rate between central bleached area and near neighbor, the fluorescence intensity of Kv4.3-GFP declined much faster in the former than the latter. These are consistent with the scenarios for proteins with high or low mobility depicted in Fig. 4A. We defined 'mobility quotient' as the ratio of mean pixel value in central bleached area to that of its near neighbor at a time point 200 s after beginning photobleaching pulses. The mobility quotients of mCherry and Kv4.3-GFP were 0.98 and 0.20, respectively.

We applied FLIP to compare the mobility of palmitoylatable and unpalmitoylatable KChIP2.2-mCherry ('WT' and C45A/C46A 'Mut') in the cytoplasmic compartment (Cyto-to-Cyto, Fig. 4C). While the fluorescence intensity of Mut declined at the same rate between the central bleached area and near neighbor, the fluorescence intensity of WT declined faster in the former than the latter. The mobility quotient of Mut was much higher than that of WT (Fig. 4F). Pretreatment with 2BP markedly accelerated WT mobility to the same level as Mut, without further increasing Mut mobility (Fig. 4F), indicating that the slower mobility of WT in cytoplasm was due to palmitoylation.

To compare WT and Mut in their nuclear entry rate (Cyto-to-Nu, Fig. 4D), the whole nuclear region was bleached and the perinuclear zone was the near neighbor. The nuclear entry rate of WT trended slower than that of Mut (Fig. 4F). To test whether the slower nuclear entry rate of WT was due to the exclusion of its palmitoylated fraction from entering the nucleus, we tested whether it could be accelerated by inhibiting palmitoylation. Indeed, pretreatment with 2BP significantly accelerated the Cyto-to-Nu mobility of WT to the same level as Mut, without changing that of Mut (Fig. 4F).

To monitor the nuclear exit rate of KChIP2.2-mCherry, fluorescence in the whole cytoplasm was bleached and fluorescence decline in the nuclear region reported nuclear exit of fluorescent molecules (Nu-to-Cyto, Fig 4E). The mobility quotients of WT and Mut in the Nu-to-Cyto direction were significantly lower than the mobility quotients in the opposite direction (Fig. 4F), indicating that KChIP2 was retained inside the nuclei once it entered. 2BP pretreatment did not accelerate the nuclear exit rate.

Fig. 4C–4F show that the palmitoylation status of KChIP2 influences its mobility: palmitoylatable KChIP2 had a lower mobility in the cytoplasm and a slower nuclear entry rate than unpalmitoylatable counterpart, while the latter could enter nuclei readily but exited nuclei very slowly. These variations in trafficking behavior are expected to contribute to the differential distribution pattern observed at steady-state (Fig. 2C).

Palmitoylatable and unpalmitoylatable KChIP2.2-mCherry expressed in cardiac myocytes exhibit differential distribution and mobility

To test how WT and C45A/C46A mutant of KChIP2.2-mCherry behave when expressed in the native myocyte environment, we used adenovirus-mediated gene transfer to express them in adult cardiac myocytes. Two cell types were used: rat ventricular myocytes and guinea pig

Author Manuscript Author Manuscript Author Manuscript Author Manuscript

atrial myocytes. They differ in two aspects: native I_{to} channels and t-tubule structures are present in rat ventricular myocytes but absent in guinea pig atrial myocytes. Comparing the distribution of the two KChIP2 variants between the two cell types enabled us to discern possible roles played by native I_{to} components (Kv4.2/Kv4.3/KChIP2 in rat myocytes) in the observed patterns, and to infer the nature of the striation pattern of native KChIP2 observed in some myocytes (Fig. 1A).

Fig. 5A depicts representative immunofluorescence images of WT and Mut in the two groups of myocytes. WT had a strong presence at PM, but dim inside nuclei. Mut was dim at PM but strong inside nuclei. The Mut signal was also stronger than that of WT in the cytoplasm. The images were quantified as % pixel contents in three ROIs: cytoplasm, cell periphery (PM) and nucleus (Fig. 5B). This differential distribution pattern was qualitatively the same between rat and guinea pig myocytes, indicating that the distribution was not dictated by the native I_{to} components in the former group.

We applied FLIP to compare the mobility of WT and Mut in rat ventricular myocytes (Fig. 5C–5E). The mobility of WT was much lower than that of Mut in Cyto-to-Cyto and Cyto-to-Nu directions. The mobility of Nu-to-Cyto was similarly low for both WT and Mut.

We further used the Palm-PLA method to label palmitoylated KChIP2 in rat ventricular myocytes. Palm-PLA signals manifested as distinct puncta in myocytes infected with adenovirus carrying KChIP2.2-mCherry and incubated with palmitate-alkyne under the control conditions (Fig. 6A). The puncta were very sparse in adenovirus-infected myocytes treated with 2BP (quantification in Fig. 6B), and not detectable in myocytes without adenovirus infection, where after 24-hr culture native KChIP2 was barely detectable by immunofluorescence (Fig. 6A). These data validate the Palm-PLA detection method applied to myocytes, and confirm that cardiac myocytes have native enzyme(s) to palmitoylate KChIP2. Furthermore, Palm-PLA puncta exclusively clustered to myocytes' lateral surface, despite abundant protein (immunofluorescence signals) in striations along the z-lines (Fig. 6A, left), confirming that palmitoylation of KChIP2 enhanced its binding to the plasma membrane in myocytes.

The above data show that the differences between palmitoylatable (WT) and unpalmitoylatable (Mut) KChIP2.2-mCherry, in terms of their PM/nucleus distribution and mobility in cytoplasm and between cytoplasm and nucleus are qualitatively the same when expressed in COS-7 cells and in cardiac myocytes. These similarities indicate that their distribution and mobility reflect their intrinsic properties driven by the palmitoylation status.

Binding of unpalmitoylated KChIP2 to palmitoylating enzyme contributes to its striation pattern in myocytes

Fig. 5A shows that the unpalmitoylatable form of KChIP2.2-mCherry exhibited prominent striations along the z-lines, resembling the striation pattern of native KChIP2 seen in some myocytes (Fig. 1A). Since this was seen in guinea pig atrial myocytes that do not have t-tubules, we conclude that the striation pattern of KChIP2 is not *solely* due to binding to the t-tubule membrane or proteins embedded in the t-tubule membrane (e.g. L-type Ca channels). Fig. 7A depicts the distribution patterns of native Kv4.3 and KChIP2 in two

Author Manuscript Author Manuscript Author Manuscript Author Manuscript

canine ventricular myocytes isolated from the same heart and processed in parallel. The localization of these two proteins was clearly dissociated. It has been shown that in rat ventricular myocytes a small percentage of Kv4.2 and KChIP2 (15% and 20% of total, respectively) is present in lipid-raft domains [23]. Kv4.2 is recruited to the lipid-raft domains by association with a scaffold protein, postsynaptic density protein 95 (PSD-95) [24], which is palmitoylatable [22]. Whether the same applies to Kv4.3 in cardiac myocytes, and whether KChIP2 and PSD-95 are differentially modulated by cellular milieu in terms of their palmitoylation status, require future investigation.

We explored three other explanations for the striation pattern of KChIP2. It has been shown that in guinea pig ventricular myocytes, presenilin-1 (PSEN1) is enriched in the junctional SR compartment [8] along the z-lines and can interact with KChIP2[5]. Fig. 7B, left, shows that in a rat ventricular myocyte where unpalmitoylatable Mut KChIP2.2-mCherry exhibited prominent striations, PSEN1 clustered to the lateral surface. Therefore, PSEN1 is not the driving force for KChIP2 to form striations.

The second possibility is that the distribution of unpalmitoylated KChIP2 may be driven by the localization of palmitoylating enzymes. It has been shown that depalmitoylated H- and N-ras proteins are directed to the Golgi for repalmitoylation [25]. A palmitoylating enzyme, DHHC5, is expressed in the rat heart [26], and coexpressing DHHC5 with KChIP2 in HEK293 cells increased the degree of KChIP2 palmitoylation (Fig. S4A). We used a DHHC5 Ab (validated for immunofluorescence detection of DHHC5, Fig. S4B) to monitor its distribution pattern in rat ventricular myocytes expressing unpalmitoylatable (Mut) KChIP2.2-mCherry. In all myocytes examined, unpalmitoylated KChIP2 was well colocalized with DHHC5 along the z-lines (one example shown in Fig. 7B, right). On the other hand, of 4 other DHHC enzymes tested (DHHC1, 2, 4 and 6), none exhibited striations along the z-lines as DHHC5 (Fig. S5). This strongly suggests that the striation pattern of native KChIP2 may reflect, at least in some myocytes, binding of depalmitoylated pool to the DHHC5 enzyme for repalmitoylation. Finally, F-actin marker, phalloidin, was well colocalized with unpalmitoylatable Mut KChIP2-mCherry in rat ventricular myocytes. The underlying mechanism and its functional implication need to be tested in future experiments.

Acute stress promotes nuclear entry of native KChIP2 in cardiac myocytes

The above data show that KChIP2's distribution pattern is largely determined by its palmitoylation status. To explore the patho-physiological correlates of these findings, we tested whether acute stress in a rat model of cardiac arrest (for 8 min) followed by cardiopulmonary resuscitation (CAR) [13] could alter KChIP2 distribution in cardiac myocytes. In control myocytes, KChIP2 was abundant in cell periphery but low in nuclei. In CAR myocytes, KChIP2 was low in cell periphery but high in nuclei (Fig. 8A and B). Immunoblot confirmed the increase in nuclear KChIP2 in acutely stressed hearts (Fig. 8C). Furthermore, KChIP2 in CAR myocytes exhibited prominent striations along the z-lines, similar to those of unpalmitoylatable Mut KChIP2.2-mCherry expressed in the same cell type (Fig. 5A). These observations indicate that the palmitoylation status and distribution pattern of native KChIP2 in cardiac myocytes are dynamic. Acute stress such as in the CAR model can trigger KChIP2 depalmitoylation and nuclear entry, diverting its role from ion

Author Manuscript Author Manuscript Author Manuscript Author Manuscript

channel modulator at the PM to transcription regulation (and potentially other functions) inside the nuclei.

DISCUSSION

Native KChIP2 in cardiac myocytes: subcellular distribution and functions

Our data suggest that native KChIP2 is distributed across five major subcellular compartments in cardiac myocytes, and the palmitoylation status is the major force driving its distribution.

1. Cell periphery: This includes the plasma membrane and a 1–2 um sub-sarcolemma space. The latter is suggested by the 'fuzzy' immunofluorescence signals within 1–2 um space from the cellular contour in confocal images (Fig. 5A, WT KChIP2.2-mCherry; Fig. 8A, native KChIP2 in the control myocyte). We suggest that this represents palmitoylated KChIP2 binding to the PM and structures beneath the PM. This is based on the observation that Palm-PLA signals in ventricular myocyte exclusively clustered here (Fig. 6A). KChIP2 present in this compartment is expected to modulate the function of cell surface channels, including Kv4 and L-type Ca channels [1, 3, 7].

2. Nucleus: We suggest that this represents depalmitoylated KChIP2 binding to structures in the nucleoplasm. The strongest support for this statement is Fig. 3: we detected the unpalmitoylated pool of KChIP2.2-mCherry inside nuclei, but not or very little of palmitoylated pool. KChIP2 inside nuclei may function as a Ca-sensitive transcription repressor like KChIP3 [2]. Indeed, it has been shown that KChIP2 can modulate the transcription of microRNAs [5].

3. Striations along the z-lines in the cytoplasm: This may represent several scenarios based on the literature: association with the L-type Ca channels [7] or Kv4 channels embedded in the t-tubule membrane, or association with presenilin-1 embedded in the junctional SR membrane [5]. Our data suggest that this mainly represents the depalmitoylated pool of KChIP2, because unpalmitoylatable (Mut) KChIP2.2-mCherry exhibited much more prominent striations than the palmitoylatable (WT) KChIP2.2mCherry (Fig. 5A), and the dim striations in the latter might represent the unpalmitoylated pool, as is suggested by the Palm-PLA signals (Fig. 6A). We further suggest that striations of depalmitoylated KChIP2 is driven by binding to a palmitoylating enzyme, DHHC5 present in the z-lines of myocytes, likely for repalmitoylation.

4. Golgi apparatus and vesicles: KChIP2 detected in perinuclear Golgi apparatus and cytoplasmic vesicles may represent KChIP2 involved in protein trafficking in myocytes. Indeed, KChIP2 is an important modulator for cell surface expression of Kv4 channels [1]. KChIP2 may also modulate cell surface expression of Kv1.5 [6]. Fig. 6A suggests that KChIP2 in this subcellular compartment may be depalmitoylated.

5. Cytosolic soluble compartment: Fig. 5A suggests that there is a pool of soluble KChIP2, mainly in depalmitoylated state, in the cytoplasm. We suggest that this

Author Manuscript Author Manuscript Author Manuscript Author Manuscript

pool was not detected in previous reports using detergent-permeabilized myocytes: the soluble/mobile pool of KChIP2 was lost, leaving KChIP2 pools retained inside nuclei or bound to cytoplasmic organelles (corroborated by live COS-7 cell imaging in Fig. S6, where cytosolic KChIP2.2-mCherry was lost 8 min after application of 0.01% Triton). Whether the soluble pool of KChIP2 is passively passing among subcellular compartments, or is actively engaging in interactions with other molecules (e.g. F-actin, Fig. 7B) requires further investigation.

Mechanism of nuclear entry of KChIP2

Our experiments suggest a mechanism contributing to the differential cytoplasmic-nuclear distributions of KChIP2. Palmitoylated KChIP2 had a lower cytoplasmic mobility than unpalmitoylated KChIP2, indicating a retention of the former in the cytoplasm. Unpalmitoylated KChIP2 had a much lower nuclear exit rate than nuclear entry rate, indicating a retention mechanism inside the nuclei. This ‘retention’ mechanism for differential distribution between cytoplasm and nucleus is similar to how β-catenin is distributed between the two compartments via an importin-independent process [27]. Proteomic studies will be undertaken to check whether KChIP2 can interact with importins in the conventional importin-mediated translocation through the nuclear pore complexes.

Conclusions

Our data suggest dynamic regulation of palmitoylation status and distribution pattern of KChIP2 in cardiac myocytes. Acute stress associated with an episode of cardiac arrest of ~ 8 min was able to promote KChIP2 translocation from cell periphery into the nuclei. This is expected to shift the role of KChIP2 from ion channel or presenilin modulation to transcription or other regulation. Further studies investigating the functional consequences of nuclear entry of KChIP2 might unveil novel roles for KChIP2 under normal and diseased conditions.

Supplementary Material

Refer to Web version on PubMed Central for supplementary material.

ACKNOWLEDGEMENTS

Confocal microscopy was performed at the Virginia Commonwealth University – Department of Anatomy and Neurobiology Microscopy Facility, supported in part by NIH-NINDS Center Core Grant 5P30NS047463.

FUNDING

This work was supported by grants from NIH/NHLBI (HL96962 to ID and GNT, HL128610 to GNT, HL132520 to ID), and by AHA Grant-in-Aid (16GRNT29920012 to GNT).

Abbreviations:

CAR	cardiac arrest/resuscitation
2BP	2-bromopalmitate

Author Manuscript Author Manuscript Author Manuscript Author Manuscript

Palm-PLA	palmitoylated detected by proximity ligation amplification
Unpalm-PLA	unpalmitoylated detected by proximity ligation amplification
PSEN1	presenilin-1

REFERENCES

[1]. An WF, Rowlby MR, Betty M, Cao J, Ling H-P, Mendoza G et al. Modulation of A-type potassium channels by a family of calcium sensors. Nature 2000;403:553–6. [PubMed: 10676964]

[2]. Spreafico F, Barski JJ, Farina C, Meyer M. Mouse DREAM/Calsenilin/KChIP3: gene structure, coding potential, and expression. Molecular and Cellular Neuroscience 2001;17:1–16. [PubMed: 11161465]

[3]. Deschenes I, Armoundas AA, Jones SP, Tomaselli GF. Post-transcriptional gene silencing of KChIP2 and Na_v β1 in neonatal rat cardiac myocytes reveals a functional association between Na dn Ito currents. J Mol Cell Cardiol 2008;45:336–46. [PubMed: 18565539]

[4]. Nassal DM, Wan X, Liu H, Maleski D, Ramirez-Navarro A, Moravec CS et al. KChIP2 is a core transcriptional regulator of cardiac excitability. eLife 2017;10.7554/eLife.17304.

[5]. Nassal DM, Wan X, Liu H, Laurita KR, Deschenes I. KChIP2 regulates the cardiac Ca^{2+} transient and myocyte contractility by targeting ryanodine receptor activity. PLoS-One 2017;12:e0175221. [PubMed: 28384221]

[6]. Li H, Guo W, Mellor RL, Nerbonne JM. KChIP2 modulates the cell surface expression of Kv1.5-encoded K^+ channels. J Mol Cell Cardiol 2005;39:121–32. [PubMed: 15878168]

[7]. Thomsen MB, Wang C, Ozgen N, Wang H-G, Rosen MR, Pitt GS. Accessory subunit KChIP2 modulates the cardiac L-type calcium current. Circ Res 2009;104:1382–9. [PubMed: 19461043]

[8]. Takeshima H, Venturi E, Sitsapesan R. New and notable ion-channels in the sarcoplasmic/endoplasmic reticulum: do they support the process of intracellular Ca^{2+} release? J Physiol 2015;593:3241–51. [PubMed: 26228553]

[9]. Levin ER, Hammes SR. Nuclear receptors outside the nucleus: extranuclear signaling by steroid receptors. Nature Reviews Molecular Cell Biology 2016;17:783–97. [PubMed: 27729652]

[10]. Drenan RM, Doupnik CA, Boyle MP, Muglia LJ, Huettner JE, Linder MR et al. Palmitoylation regulates plasma membrane-nuclear shuttling of R7BP, a novel embrane anchor for teh RGS7 family. J Cell Biol 2005;169:622–33.

[11]. Liao P, Wang W, Li Y, Wang R, Jin J, Pang W et al. Palmitoylated SCP1 is targeted to the plasma membrane and negatively regulates angiogenesis. eLife 2017;6:e22058. [PubMed: 28440748]

[12]. Takimoto K, Yang E-K, Conforti L. Palmitoylation of KChIP splicing variants is required for efficient cell surface expression of Kv4.3 channels. J Biol Chem 2002;277:26904–11. [PubMed: 12006572]

[13]. Ma L, Lu X, Xu J, Sun S, Tang W. Improved cardiac and neurologic outcomes with postresuscitation infusion of cannabinoid receptor agonist WIN55,212–2 depend on hypothermia in a rat model of cardiac arrest. Crit Care Med 2014;42:e42–e48. [PubMed: 24346544]

[14]. Jiang M, Wang Y-H, Tseng G-N. Adult ventricular myocytes segregate KCNQ1 and KCNE1 to keep the IKs amplitude in check until when larger IKs is needed. Circ Arrhythm Electrophysiol 2017;10:e005084. [PubMed: 28611207]

[15]. Hong T-T, Shaw RM. Cardiac T-tubule microanatomy and function. Physiol Rev 2017;97:227–52. [PubMed: 27881552]

[16]. Kolb HC, Finn MG, Sharpless KB. Click chemistry: diverse chemical function from a few good reactions. Agnew Chem Int Ed Engl 2001;40:2004–21.

[17]. Gao X, Hannoush RN. Method for cellular imaging of palmitoylated proteins with clickable probes and proximity ligation applied to Hedgehog, tubulin, and Ras. Journal of American Chemical Society 2014;136:4544–50.

Author Manuscript Author Manuscript Author Manuscript Author Manuscript

[18]. Kuo H-C, Cheng C-F, Clark RB, Lin JJC, Lin JLC, Hoshijima M et al. A defect in the Kv channel-interacting protein 2 (KChIP2) gene leads to a complete loss of Ito and confers susceptibility to ventricular tachycardia. Cell, 2001;107:801–13. [PubMed: 11747815]

[19]. Deschenes I, DiSilvestre D, Juang GJ, Wu RC, An WF, Tomaselli GF. Regulation of Kv4.3 current by KChIP2 splice variants. A component of native cardiac Ito? Circulation 2002;106:423–9. [PubMed: 12135940]

[20]. Landsberger M, Staudt A, Choudhury S, Trimpert C, Herda LR, Klingel K et al. Potential role of antibodies against cardiac Kv channel-interacting protein 2 in dilated cardiomyopathy. Am Heart J 2008;156:92–9. [PubMed: 18585502]

[21]. Jennings BC, Nadolski MJ, Ling Y, Baker MB, Harrison ML, Deschenes RJ et al. 2-bromopalitate and 2-(2-hydroxy-5-nitro-benzylidene)-benzo[b]thiophen-3-one inhibit DHHC-mediated palmitoylation in vitro. J Lipid Res 2009;50:233–42. [PubMed: 18827284]

[22]. Fukata Y, Murakami T, Yokoi N, Fukata M. Local palmitoylation cycles and specialized membrane domain organization. Current topics in membranes 2015;77:97–141. [PubMed: 26781831]

[23]. Rudakova E, Wagner M, Frank M, Volk T. Localization of Kv4.2 and KChIP2 in lipid rafts and modulaiton of outward K^+ currents by membrane cholesterol content in rat left ventricular myocytes. Pflugers Arch 2015;467:299–309. [PubMed: 24793047]

[24]. Wong W, Schlichter LC. Differential recruitment of Kv1.4 and Kv4.2 to lipid rafts by PSD-95. J Biol Chem 2004;279:444–52. [PubMed: 14559911]

[25]. Rocks O, Peyker A, Kahms M, Verveer PJ, Koerner C, Lumbierres M et al. An acylation cycle regulates localization and activity of palmitoylated Ras isoforms. Science 2005;307:1746–52. [PubMed: 15705808]

[26]. Howie J, Reilly L, Fraser NJ, Walker JMV, Wypijewski KJ, Ashford MLJ et al. Substrate recognition by the cell surface palmitoyl transferase DHHC5. PNAS 2014;111:17534–9. [PubMed: 25422474]

[27]. Krieghoff E, Behrens J, Mayr B. Nucleo-cytoplasmic distribution of β-catenin is regulated by retention. Journal of Cell Science 2006;119:1453–63. [PubMed: 16554443]

Author Manuscript Author Manuscript Author Manuscript Author Manuscript

- The literature shows that KChIP2 can serve different functions depending on its subcellular localization.
- Palmitoyl cycles control KChIP2 trafficking between plasma membrane and nucleus.
- Acute stress triggers nuclear entry of KChIP2 in cardiac myocytes.
- Nuclear entry diverts KChIP2's role from channel modulation to other functions inside nucleus.

Author Manuscript Author Manuscript Author Manuscript Author Manuscript

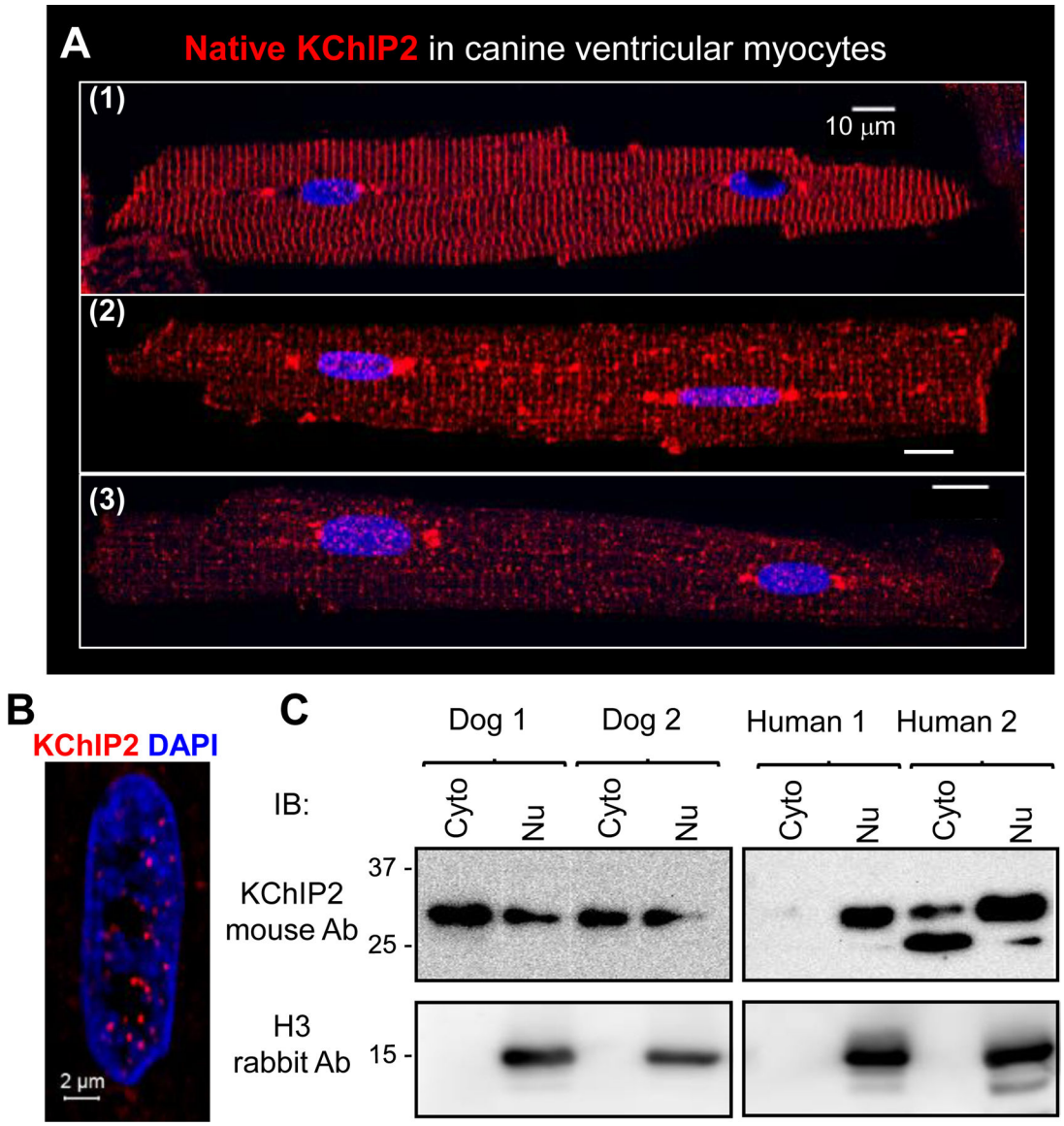

Fig. 1. Native KChIP2 in ventricular myocytes exhibits divergent distribution patterns.

(A) Immunofluorescence images of KChIP2 in three canine ventricular myocytes. **(B)** KChIP2 as distinct puncta inside a myocyte nucleus. **(C)** Immunoblot (IB) images of cytosolic (including cellular membrane) and nuclear fractions from two dog and two non-failing human hearts probed with KChIP2 mouse Ab and histone H3 rabbit Ab (nuclear marker).

Author Manuscript Author Manuscript Author Manuscript Author Manuscript

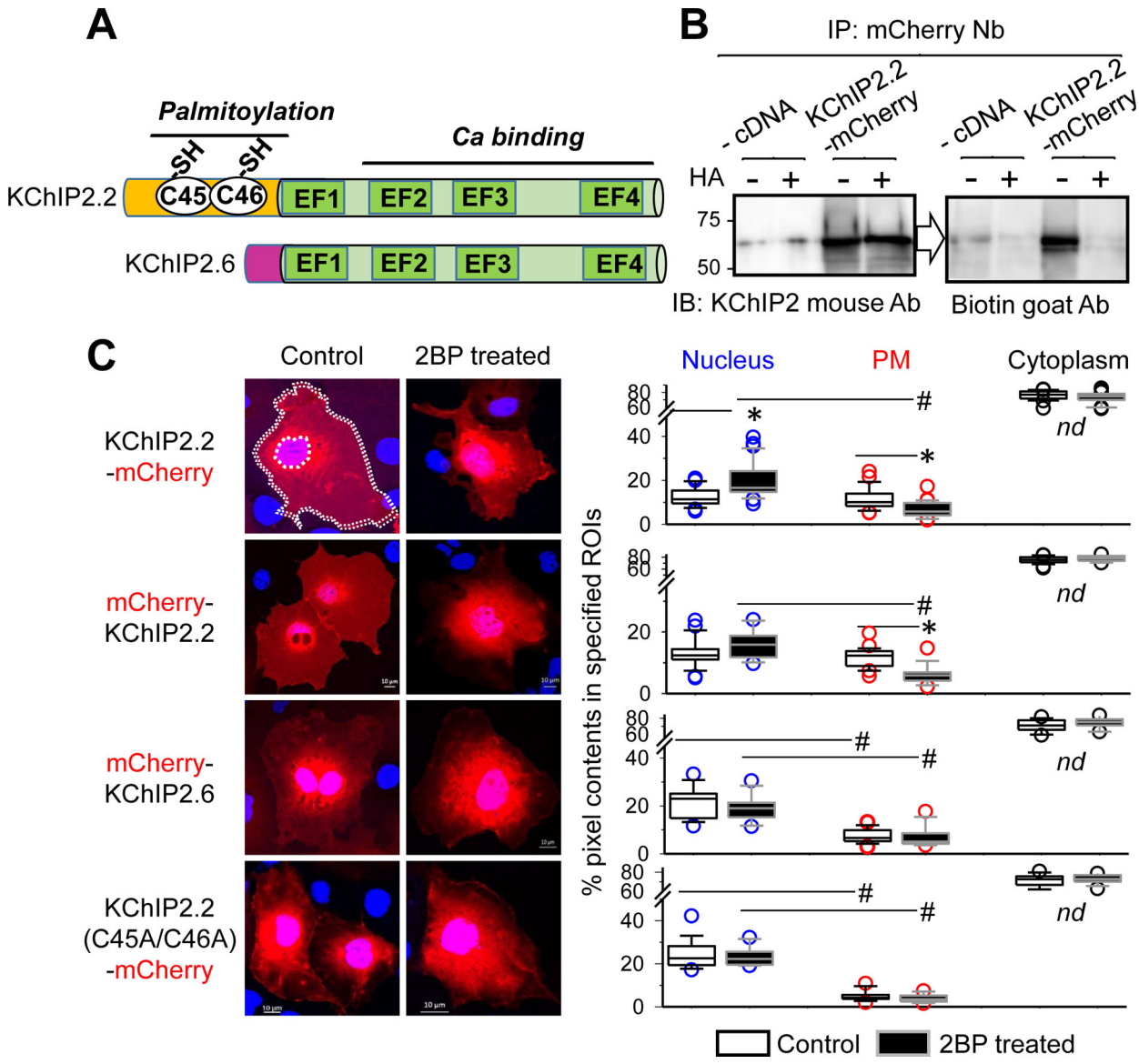

Fig. 2. The palmitoylation status of KChIP2 is a major determinant of its plasma membrane (PM)-nucleus distribution.

(A) Domain structure of splice variants, KChIP2.2 and KChIP2.6. A palmitoylation motif (C45/C46) is present in KChIP2.2, but not KChIP2.6. Both have Ca-binding EF-hand motifs (EF2-EF4). **(B)** KChIP2.2-mCherry is S-palmitoylatable. Experimental procedures are described in Fig. S1A. Untransfected (-cDNA) HEK293 cells processed in parallel served as negative control. Palmitoylated (i.e. biotinylated) KChIP2.2-mCherry was detected first by KChIP2 mouse Ab and, after stripping, by biotin goat Ab. Hydroxylamine treatment (+HA) to break thioester bonds between palmitate and Cys thiol side chain abolished the signal of palmitoylated KChIP2. **(C)** Localization of KChIP2 variants to nucleus, PM and cytoplasm in COS-7 cells under control conditions and after incubation with 2-bromopalmitate (2BP, 100 uM, 6 hr). *Left columns*: Fluorescence images of mCherry-tagged KChIP2 variants in control or after 2BP treatment. To accurately quantify the distribution of mCherry fluorescence among subcellular compartments, the images were acquired at an optical

Author Manuscript Author Manuscript Author Manuscript Author Manuscript

thickness of 2 um focused on the footprint of COS-7 cells (average cytoplasmic thickness ≤ 2 um). In this and following figures, nuclei were stained blue with DAPI or Hoechst dye. White dotted lines in the upper left panel illustrate regions of interest (ROIs): nucleus, cytoplasm and PM, the latter as 1 um wide area within the cell contour. *Right columns*: Box plots of percentage of pixel contents in specified ROIs. Data were pooled from 12 – 31 cells per group from two independent experiments. Statistics for each panel: one-way ANOVA, $p < 0.001$, Dunn's all-pairwise tests. * $p < 0.05$, control vs 2BP-treated, # $p<0.05$ nucleus vs PM. Pixel contents in cytoplasm were much higher than those in nucleus or PM, with no difference (nd) between control and 2BP-treated cells.

Author Manuscript Author Manuscript Author Manuscript Author Manuscript

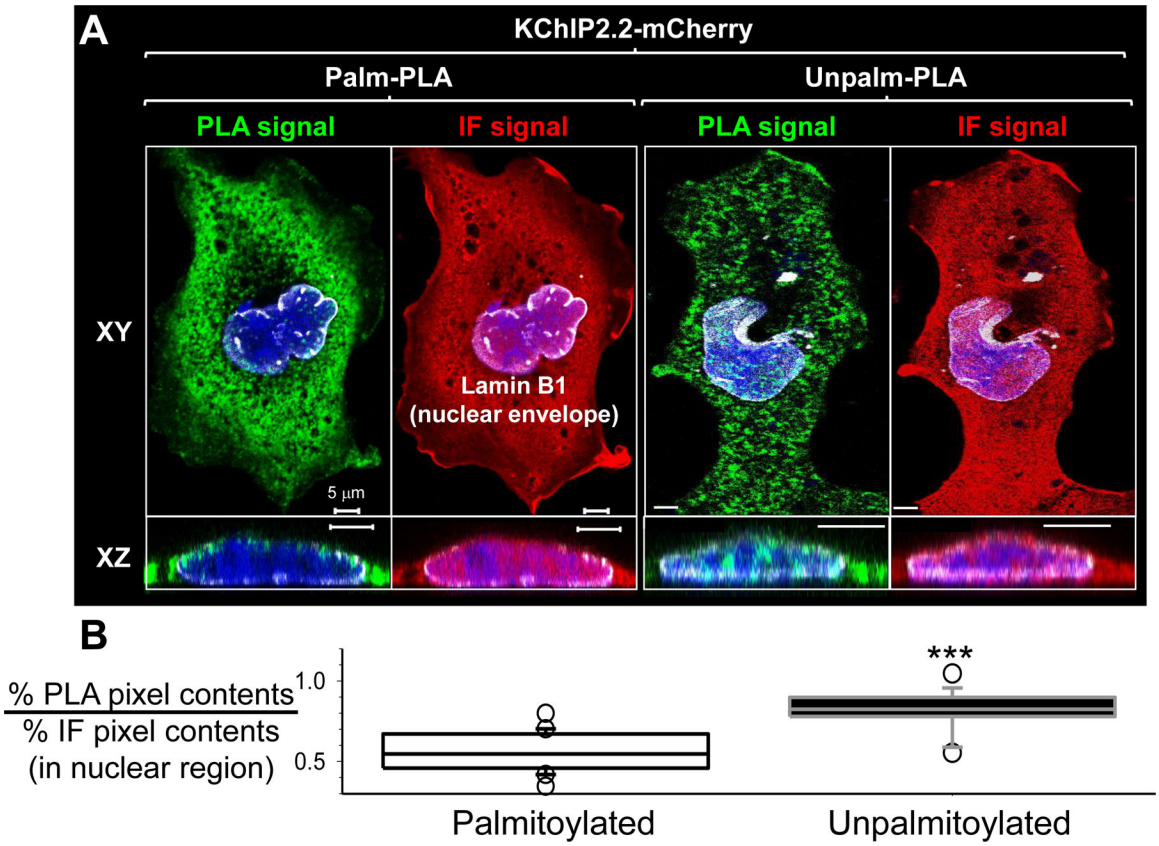

Fig. 3. Detecting palmitoylated and unpalmitoylated WT KChIP2.2-mCherry using *in situ* proximity ligation amplification (PLA).

The Palm- and Unpalm-PLA procedures are described in Fig. S1B. **(A)** Green fluorescence (PLA signals) and red immunofluorescence (IF, representing total KChIP2.2-mCherry) in the same cells viewed by 3D confocal microscopy (optical thickness 0.7 um). XY-plane: whole cell view. XZ plane: nuclear view. Lamin B1 IF (white) marks nuclear envelope. **(B)** Box plots of % PLA pixel contents in nuclear region divided by % IF pixel contents in the same region. We quantified total PLA and IF pixel contents per cell using z-projections of sum of fluorescence intensities. Using Lamin B1 signal to define ROI, we calculated % PLA or IF pixel contents in nuclear region. The PLA intensity in nuclear region corrected for difference in amount of nuclear KChIP2.2-mCherry was defined by % PLA pixel contents divided by % IF pixel contents.

Author Manuscript Author Manuscript Author Manuscript Author Manuscript

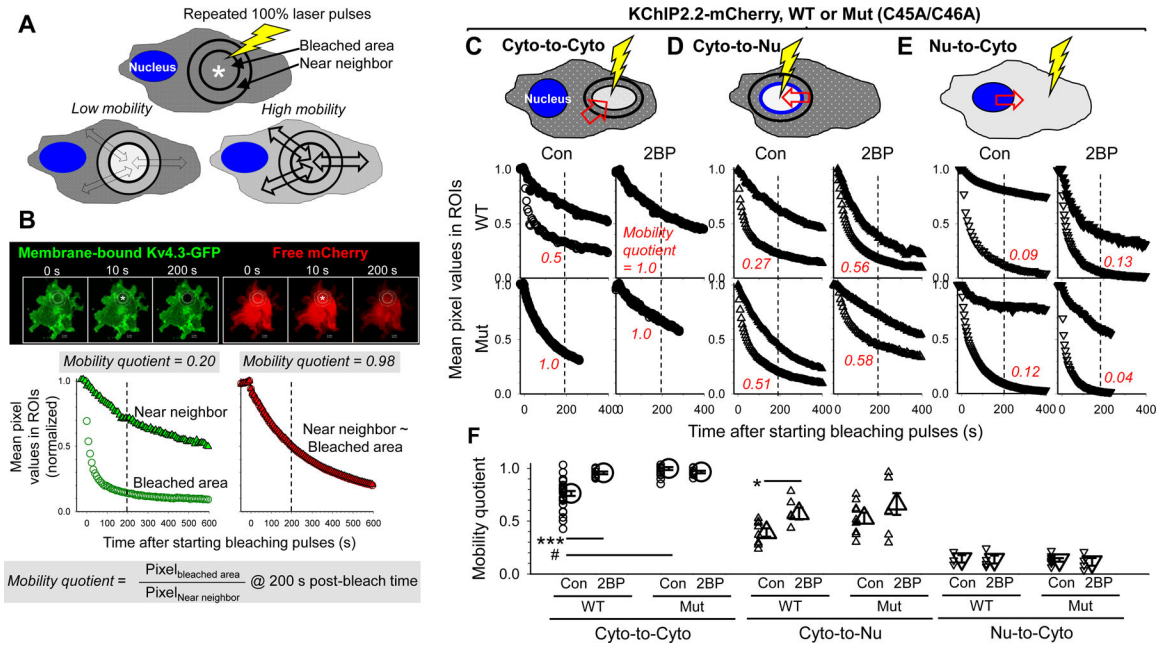

Fig. 4. Palmitoylation influences KChIP2's mobility within and between cytoplasmic and nuclear compartments.

(A) Concept of fluorescence loss in photobleaching (FLIP). *Top*: diagram of bleached area and its near neighbor. *Bottom*: two scenarios for proteins with low or high mobility. **(B)** Validation of FLIP and calculation of 'mobility quotient'. Kv4.3-GFP and free mCherry were coexpressed and analyzed by FLIP applied to the same ROIs. *Top*: fluorescence images at 0, 10 and 200 s after starting bleaching pulses (* bleached areas). *Bottom*: Time courses of changes in mean pixel values in ROIs. Dotted lines denote 200 s after starting bleaching pulses. The 'mobility quotient' is calculated as the ratio of mean pixel value in bleached area to that of near neighbor at 200 s. **(C)-(E)** Mobility of WT or Mut (C45A/C46A) KChIP2.2-mCherry within cytoplasm (Cyto-to-Cyto) and between cytoplasm and nucleus (Cyto-to-Nu and Nu-to-Cyto) in control (Con) cells or after 2BP pretreatment (2BP). *Top row*: Cartoons depicting ROIs and direction of movement of fluorescent molecules. *Bottom rows*: Time courses of decline in fluorescence intensity of directly bleached area and its neighbor, with 200 s time points and mobility quotients marked. **(F)** Mobility quotients of WT and Mut in the noted direction of movement in Con and 2BP-treated cells, and statistical analysis. Shown are individual data points (small symbols) and the mean (large symbol) with SE bar of each group pooled from up to 4 independent experiments. One-way ANOVA, $p < 0.001$, Dunn's all-pairwise comparison, * $p < 0.05$, *** $p < 0.001$, Con vs 2BP; # $p<0.001$, WT vs Mut. On-line videos show time-lapse images of mobility tests of WT in control cells (videos #1 and #2), WT in 2BP-preteated cells (videos #3 and #4), Mut in control cells (Videos #5 and #6) and Mut in 2BP-pretreated cells (videos #7 and #8).

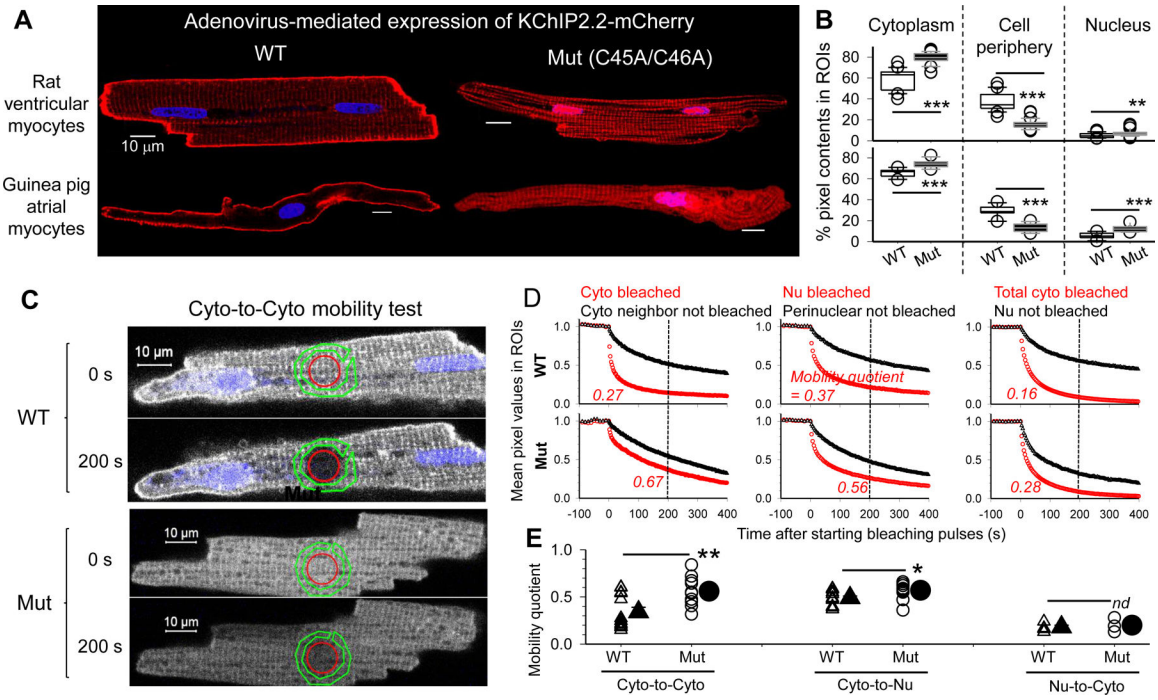

Fig. 5. WT and C45A/C46A mutant of KChIP2.2-mCherry expressed in adult cardiac myocytes exhibit distinctly different distribution patterns and mobilities.

(A) Immunofluorescence images of WT and Mut in rat ventricular myocytes and guinea pig atrial myocytes. **(B)** Box plot of % pixel contents in specified ROIs: cytoplasm, cell periphery (PM, 2 um wide area within the myocyte contour), and nucleus. **(C) – (E)** Mobility tests of WT and Mut in rat ventricular myocytes using FLIP. ROIs were delineated in the same manner as depicted in the diagrams of Fig. 4C–4E. (C) shows an example of Cyto-to-Cyto mobility test of WT and Mut. Shown are fluorescence images of live myocytes right before (0 s), and 200 s after starting bleaching pulses. ROIs are noted: red circles were directly bleached, areas delineated by green polygons were near neighbors not directly bleached. (D) shows time courses of decline in mean pixel values in ROIs, with 200 s time point and mobility quotients marked. (E) Mobility quotients of WT and Mut in the noted direction of movement in myocytes. Shown are individual data points (small symbols) and the mean (large symbol) with SE bar. Data of Cyto-to-Cyto and Cyto-to-Nu groups are pooled from 11 to 14 measurements of 2 independent experiments. Nu-to-Cyto data are from 1 experiment. Two-way t-test, WT vs Mut, ** $p < 0.01$, * $p < 0.05$; ‘nd’ no difference. On-line videos show time-lapse images of mobility tests of WT in Cyto-to-Cyto, Cyto-to-Nu and Nu-to-Cyto directions (videos #9 – #11) and Mut in Cyto-to-Cyto, Cyto-to-Nu and Nu-to-Cyto directions (videos #12 – #14).

Author Manuscript Author Manuscript Author Manuscript Author Manuscript

Author Manuscript Author Manuscript Author Manuscript Author Manuscript

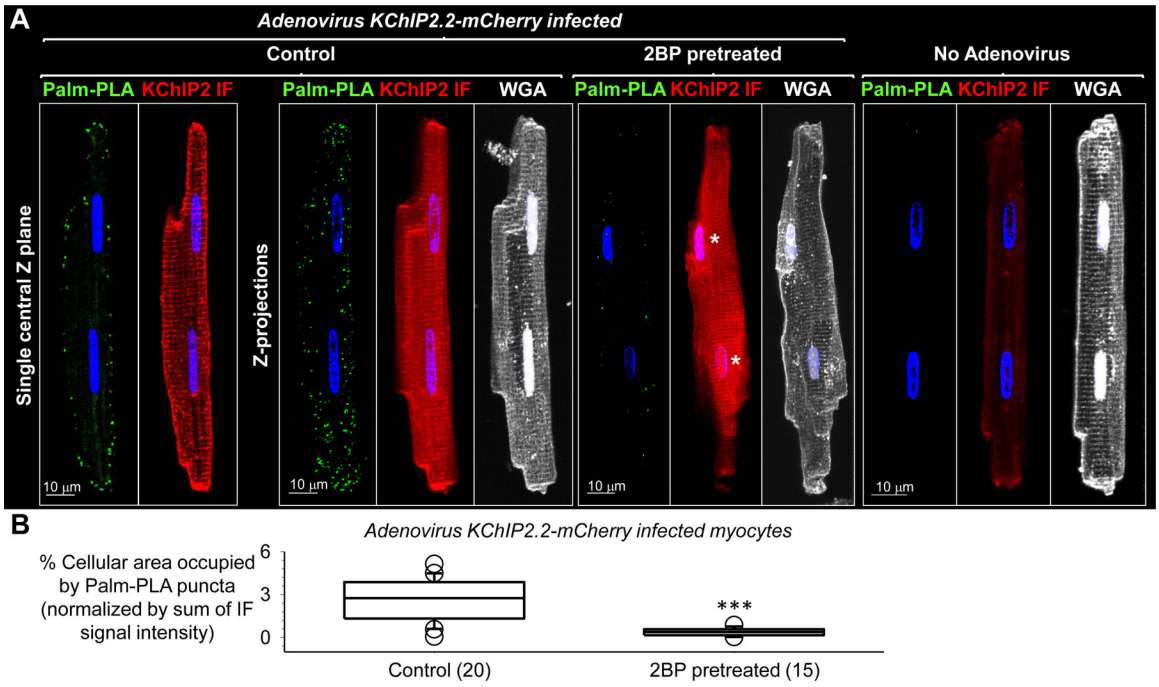

Fig. 6. Detecting distribution pattern of palmitoylated KChIP2 in cardiac myocytes and methodology validation.

Rat ventricular myocytes were incubated with adenovirus carrying KChIP2.2-mCherry for 12 hr and then with palmitate-alkyne (100 uM) under the control conditions or in the presence of 2BP (100 uM) for another 12 hr, followed by the Palm-PLA procedure. Myocytes from the same batch without adenovirus infection but otherwise processed in parallel were included for comparison. Z-stack images of Palm-PLA (green), KChIP2 IF (red) and Alexa647 wheat germ agglutinin (WGA, marker of PM and nuclear envelope, pseudo-colored white) were collected. **(A)** *Left most panels:* Single Z-plane images of Palm-PLA and KChIP2 IF from the central plane of an adenovirus-infected myocyte incubated with palmitate-alkyne under the control conditions. Palm-PLA signals manifest as distinct puncta on myocyte periphery, despite abundant KChIP2 IF signals in the cytoplasm. To quantify Palm-PLA puncta, z-projections of maximal Palm-PLA signals were subject to particle analysis in ImageJ to calculate % cellular area occupied by puncta. These value were divided by the z-projections of sum of IF signals to correct for differences in total KChIP2.2-mCherry protein level among myocytes. This process is presented in a graphical manner in Fig. S3. The remaining of (A) shows Z-projection images of Palm-PLA, KChIP2 IF, and WGA in 3 myocytes. The Palm-PLA signals are very sparse in the 2BP-preteated myocyte. Asterisks point to KChIP2 IF in nuclei of the 2BP-treated myocyte, confirming increased depalmitoylation of KChIP2.2-mCherry, corroborating the decrease in Palm-PLA signals. The Palm-PLA signal was not detectable in the myocyte without adenovirus infection, where native KChIP2 IF was barely detectable. **(B)** Box plot of Palm-PLA puncta quantification in control and 2BP-preteated myocytes. Numbers of myocytes analyzed are in parentheses (from one experiment). T-test, *** $p < 0.001$. The same pattern of Palm-PLA signals was seen in 25 adenovirus-infected myocytes incubated with palmitate-alkyne under the control conditions in two other independent experiments.

Author Manuscript Author Manuscript Author Manuscript Author Manuscript

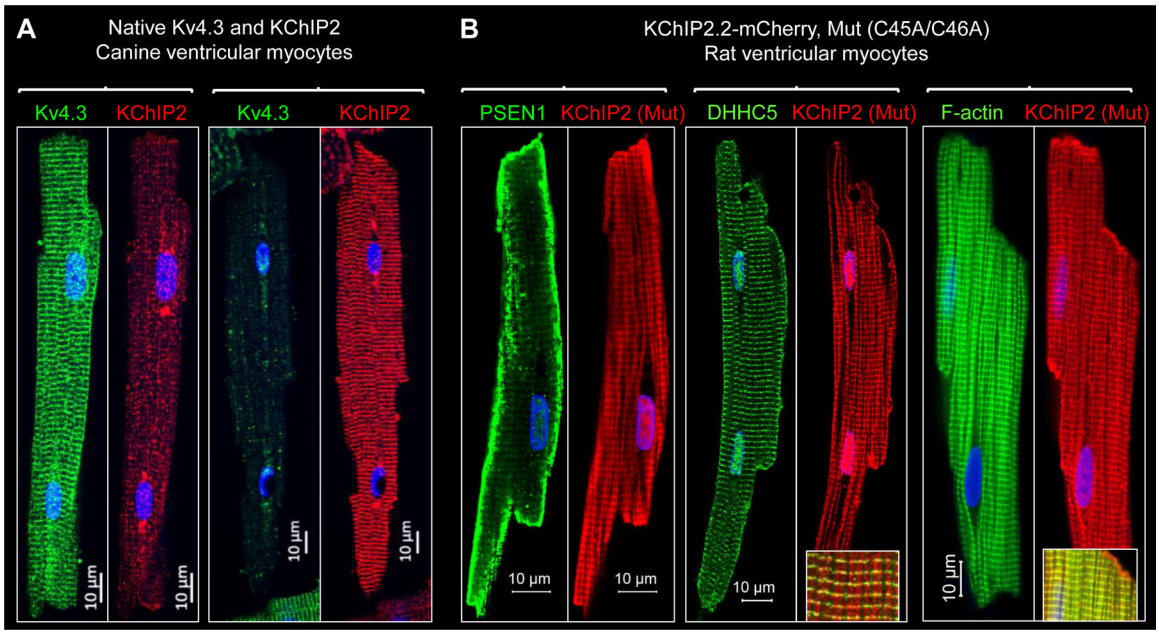

Fig. 7. Comparison of distribution patterns of KChIP2 and potential interacting proteins in ventricular myocytes.

(A) Lack of correlation between native Kv4.3 and KChIP2 in two canine ventricular myocytes. **(B)** Native presenilin-1 (PSNE1), DHHC5 (palmitoylating enzyme) and F-actin in rat ventricular myocytes expressing C45A/C46A mutant of KChIP2.2-mCherry. KChIP2 was detected by a mouse Ab/Alexa568 anti-mouse. PSEN1 and DHHC5 were detected by rabbit Abs/Alexa488 anti-rabbit, and F-actin by Alexa488 phalloidin. *Insets*: Merge of DHHC5 or phalloidin with KChIP2 signals.

Author Manuscript Author Manuscript Author Manuscript Author Manuscript

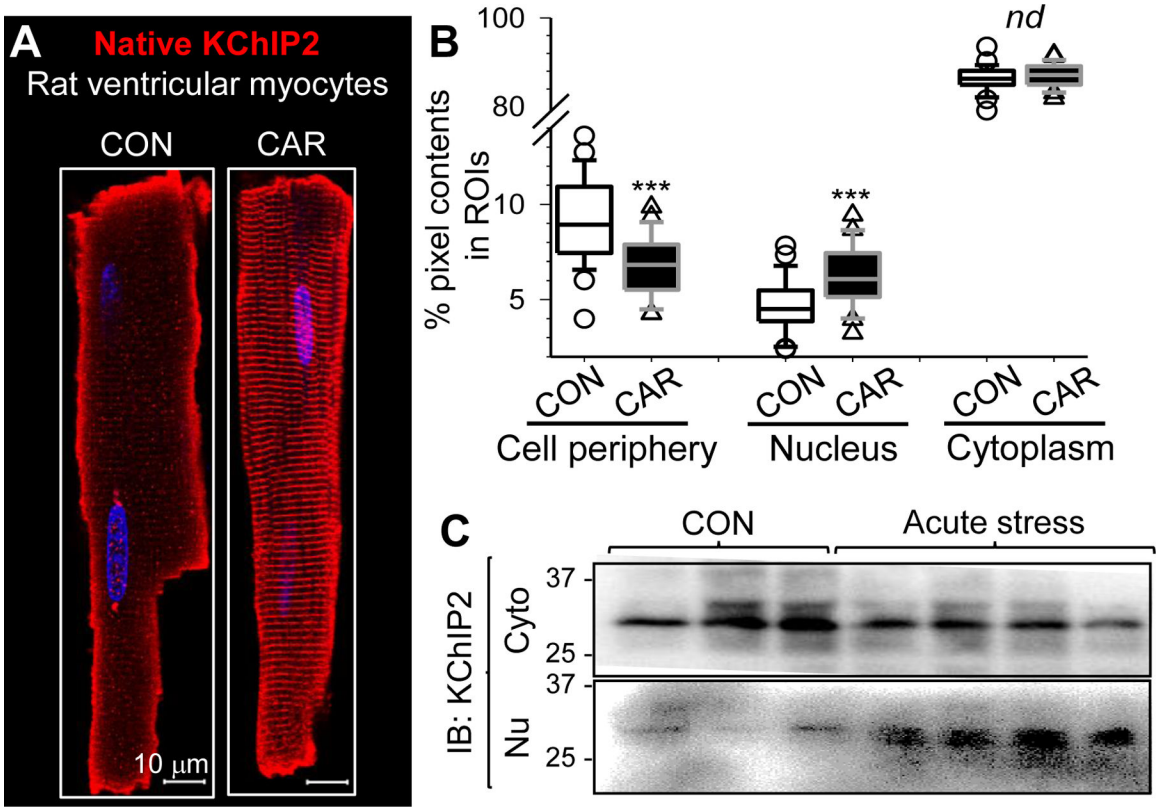

Fig. 8. In vivo stress induces nuclear entry of native KChIP2 in cardiac myocytes.

(A) Immunofluorescence images of native KChIP2 in ventricular myocytes from control rat (CON) and rat subject to acute stress (cardiac arrest for 8 min, followed by cardiopulmonary resuscitation, 'CAR'). (**B**) Box plot of % pixel contents in specified ROIs. Data are pooled from 27 CON myocytes (two animals) and 25 CAR myocytes (3 animals). Two-way t-test, CON vs CAR, *** $p < 0.001$. **(C)** Immunoblot image of native KChIP2 in cytosolic/membrane and nuclear fractions from left ventricles of animals specified on top.